RESEARCH PAPER

Acta Neurobiol Exp 2022, 82: 106–119
DOI: 10.55782/ane-2022-010

since 1928 ACTA NEUROBIOLOGIÆ EXPERIMENTALIS

Optical coherence tomography reveals heterogeneity of the brain tissue and vasculature in the ischemic region after photothrombotic stroke in mice

Hubert Doleżyczek[1], Piotr Kasprzycki[2], Jakub Włodarczyk[1], Maciej Wojtkowski[2,3,4], Monika Malinowska[1]*

[1] Nencki Institute of Experimental Biology, Polish Academy of Sciences, Warsaw, Poland,
[2] Institute of Physical Chemistry, Polish Academy of Sciences, Warsaw, Poland,
[3] International Center for Translational Eye Research, Warsaw, Poland,
[4] Faculty of Physics, Astronomy and Informatics, Nicolaus Copernicus University, Torun, Poland,
** m.malinowska@nencki.edu.pl*

We demonstrate *in vivo* imaging of the ischemic area in the mouse brain after photostroke using a custom prototype Gaussian-beam optical coherence tomography (OCT) setup in which the near infrared imaging beam and the green photoinducing light pass through the same objective lens. The goal of our research was analysis of vascularity of the ischemic area during 2-week progress of stroke and correlating the hypo- and hyperreflective OCT scattering areas with the location of activated microglia and astroglia. Angiogenesis, which was assessed using angiomaps, showed that the area of vessels in the ischemic center increased until day 7. OCT imaging revealed a heterogeneous scattering signal pattern in the ischemic area. On structural OCT images, we found presence of a core area of ischemia with a hyporeflective OCT signal and a halo of hyperreflective signal around the core. The core signal decreased in size by 70% by day 14. Immunocytochemistry revealed that the hyporeflective area in the ischemic core was associated with microglia/macrophage activation, whereas the hyperreflective signal from the halo came from activated astrocytes.

Key words: optical coherence tomography, stroke, ischemic region, glia, mice

INTRODUCTION

Optical coherence tomography (OCT) is a non-invasive technique for three-dimensional imaging of biological samples. It is based on the detection of infrared light scattered back from living tissue. OCT has been adopted in the clinic for diagnostic visualization of the diseased eye. For example, it has been used for diagnostic visualization in macular degeneration (Hee et al., 1996), glaucoma and diabetic retinopathy (Deissaire et al., 2020). Recently, OCT has been widely applied in the visualization of brain pathomorphology observed during *ex vivo* imaging of β-amyloid in Alzheimer's disease (Baumann et al., 2017), and glioblastoma structure (Gesperger et al., 2020) as well as during *in vivo* imaging (through the cranial window) of glioblastoma (Yecies et al., 2019; Doleżyczek et al., 2020a) and stroke (Yang et al., 2018; Choi et al., 2019). In previous studies (Doleżyczek et al., 2020b), we demonstrated the usefulness of OCT in brain imaging 24 h after stroke. In the present work we have shown that our new modified OCT system is a valuable tool for detailed analysis of vascularity ischemic area over the course of 2 weeks. The literature also describes changes in vascularity in a shorter time, up to a few days (Choi et al., 2019; Sunil et al., 2021; Lee et al., 2019).

Cerebral ischemic stroke is caused by clot formation in the arterial lumen, which restricts blood supply to distal parts of the brain and ultimately leads to

Received 24 September 2021, accepted 26 January 2022

neuronal cell death in the ischemic area, resulting in neurological deficits in learning/memory and motor deficits (Bosetti et al., 2017). Photothrombotic stroke is widely applied in animal models of ischemic stroke (Yang et al., 2018; Doleżyczek et al., 2020b). In this model, the animal is administered a photosensitive agent Bengal Rose (BR) that reaches the bloodstream. Then the selected area of the brain is irradiated with light with a wavelength of about 562 nm (max of absorption), which activates the BR. The resulting oxygen free radicals damage the vascular endothelium, which causes local adhesion and aggregation of platelets forming clots. Brain regions deprived of blood perfusion alter their tissue and cellular structure. Ischemia induces excitotoxicity and inflammatory processes with neuronal necrosis/apoptosis, and activation and migration of astrocytes and microglia (Lee at al., 2018). Also, brain edema, which results from damage to the blood-brain barrier, causes impairment of the brain nervous tissue. Degenerated neurons and damaged tissue have been shown to be scavenged by activated microglia (phagocytic microglia) and/or macrophages that migrate to the ischemic tissue from the bloodstream (Margaritescu et al., 2009). With the transient middle cerebral artery occlusion stroke model, phagocytic microglia were present from day 1 up to day 14. Quantitative analysis revealed maximum numbers of local-origin phagocytic microglia within 2 days and of blood-borne macrophages on day 4 (Schilling et al., 2005).

The ischemic region has a heterogeneous structure consisting of the ischemic core (infarct) characterized by irreversible neuronal necrosis surrounded by the ischemic penumbra. The penumbra is perfused to a level that partially prevents functional damage and morphological disintegration, and it has the ability to regenerate if perfusion is improved (Paciaroni et al., 2009). Both the infarct and penumbra volumes change over time, the penumbra-infarct ratio decreases, and eventually, the penumbra disappears days or weeks after stroke (Dirnagl et al., 1999). In the penumbra and surrounding tissue, activated astrocytes with microglia form a glial scar that separates the necrotic area from normal nervous tissue (Zbesko et al., 2018). The impact of these structural rearrangements in the ischemic brain area on the scattering properties of the tissue is what makes OCT visualizations an advantageous tool for analyses of murine brain after stroke observed *in vivo* (Yang et al., 2018) as well as *ex vivo* (Osiac et al., 2014). Observed alterations in the blood vessel network occur in parallel to the nervous tissue impairment. In the first days after the stroke, some of the vessels (especially capillaries) degenerate. To restore the physiological functions of ischemic brain tissue, it is necessary to improve the circulation as soon as possible. On the one hand, spontaneous reperfusion occurs in some small arterioles. However, the most important process after stroke is the formation of new microvessels (angiogenesis) (Hatakeyama et al., 2020). The extent of angiogenesis determines the size of the damaged tissue and the recovery time. Many studies have shown that the OCT method is useful in assessing cerebral vascularization (Srinivasan et al., 2013; Tamborski et al., 2016; Park et al., 2018).

In this work, we demonstrate another significant step in the development of optical imaging techniques for mouse brain imaging in a stroke model achieved by longitudinal observation of the evolution of post-stroke lesions. In order to analyze the structure of the ischemic area and angiogenesis, we performed OCT imaging within 2 weeks after the stroke, followed by histological staining of the nervous tissue cells. We identify a new source of information in the form of hypo- and hyperreflective areas on OCT images that may serve in the future as biomarkers in monitoring of therapies and observation of impacts of strokes. We also provide a physiological interpretation of the origin of these changes present in the OCT reconstructions.

METHODS

Experimental setup, scanning protocol and data processing

Fig. 1S presents the multifunctional and multimodal device used in this study. The OCT system allows three-dimensional structural and angiographic imaging of ischemic brain regions, and the brightfield microscope channel allowed precise animal positioning and real-time imaging of superficial vessels. Here, a spectral OCT system of our own design based on a Michelson interferometer configuration using a Gaussian beam was used. Briefly, a commercial Semiconductor Optical Amplifier (SUPERLUM M-T-850-HP-I) with a wavelength of 850 nm and a bandwidth of at least 155 nm (providing an axial resolution of 2.2 μm) was used for OCT scanning along with a 75:25 fiber optic splitter to split the amplitude of input light into a reference and object arm, respectively. The light reflected from the sample and the reference mirror was coupled using the same fiber optic coupler and directed to the spectrometer. The interferometric signal was recorded by a custom-made spectrometer (diffraction grating, 1200 lp/mm; Wasatch Photonics, Morrisville, North Carolina, USA) with a high-speed 2048-pixel linear scanning camera (Basler Sprint, Ger-

many). Interchangeable imaging optics can be used with the OCT system; however, in this study we used a 4x microscope objective (Olympus Plan Fluorite, 4X/0.13, full aperture equivalent = 11.7 mm, effective focal length = 45 mm, working distance = 17 mm). To achieve a trade-off between lateral resolution and depth of field, the beam entering the lens was extended to 6 mm (at $1/e^2$ of Gaussian profile) through the achromatic f=+30 mm and f=+100 mm lenses. The theoretically estimated confocal parameter is ~100 μm for an acquired lateral resolution of Δx=4.5 μm (at the FWHM of the Gaussian profile). The sample was illuminated with a scanning beam of 0.6 mW average optical power. Lateral laser beam scanning was accomplished using a pair of galvo-scanners (Cambridge Technology, Bedford, Massachusetts, USA). A-scans were collected at 50 kHz repetition rate. Three-dimensional volumes covering an area of 1.4 mm × 1.4 mm × 2 mm were acquired with sampling density of 400 × 400 × 2048 pixels for X, Y and Z axes, respectively. Imaging depth limited by the light penetration and multiple scattering was estimated to 450 μm. At each position along the Y-axis, the B-scans were repeated six times with a repetition time of 8.2 ms. The six repeated frames were used to calculate angiographic cross-sections, or averaged to improve the quality of the OCT structure images. Full three-dimensional volume was collected within 19.2 s, but total measurement time, including data transfer and saving, was 94 s. Dedicated stand-alone software, developed in LabVIEW, allowed the control of a scanning protocol, synchronization of camera and scanners, and data processing. Data analysis enabled volumetric reconstruction of mouse brain structure and angiographic mapping. Angiographic analysis was carried out according to the procedure described elsewhere (Doleżyczek et al., 2020a). The brightfield microscope was coupled to the OCT system using a dichroic mirror. The lens system, coupled to a manually-focused charge coupled device (CCD) camera lens (Thorlabs), allowed precise positioning of the animals relative to the scanning beam. A third part of the system, for local photoinduction, shared part of the optical path with the brightfield microscope and was connected to the OCT microscope using the same dichroic mirror. A laser diode (Thorlabs) with a wavelength of 520 nm and a power of 1.1 mW was used for photoactivation.

Animals

All procedures were performed according to the rules established by the First Local Ethical Committee on Animal Research in Warsaw (permission no 986/2020). These rules are based on national laws in full accordance with the European Union directive on animal experimentation.

Cranial window installation

Twelve certified female FVB mice (age=8-10-months; weight=20-25 g) were used in the experiments. Photochemical stroke was induced in all of the mice. Two of the mice were excluded due to technical failure. The mice were prepared for imaging by implanting a cranial window. This technique was described in detail previously (Doleżyczek et al., 2020b). During the procedure, animals were anesthetized with isoflurane. Dexamethasone (0.2 mg/kg) and Carprofen (5 mg/kg) were administered subcutaneously to prevent an inflammatory response and brain edema. After removal of the skin at the top of the skull, a circular section of the skull (diameter 4 mm) was removed to expose the dura. The dura mater was removed, and the surface of the brain was covered with 0.9% NaCl. Then, a cover glass (diameter 5 mm) was attached to the skull with cyanoacrylate-based glue and sealed with dental acrylic. After the surgical procedure, the mice were transferred to cages and monitored until total recovery.

Stroke induction and *in vivo* OCT brain imaging

Four weeks after cranial window implantation, OCT measurements were performed in 10 mice. Each animal was placed in a stereotaxic frame with a warming pad and deeply anaesthetized with isoflurane (4% for induction; 1.5–2% for the procedure). The stereotaxic frame was then positioned in the OCT setup using a custom-made three-axis platform. Access to the animal's brain was possible due to the extended focus of the imaging system. The long working distance (7.5 mm) of the 4x lens allowed for comfortable positioning of the animal. To induce focal photoactive stroke, BR 100 mg/kg body weight in saline (25 mg/ml) was administered intraperitoneally. Then, after 5 min, when the BR dye reached the blood circulation, photoactivation was initiated using a 520-nm laser diode beam focused on the area between the larger branches of the medial cerebral artery (MCA), located about 2 mm posterior to the bregma. The beam diameter was 400 μm. Cortex illumination continued for 20 min (Fig. 2SA). In each following time point, a single three-dimensional OCT volume was acquired: 5 min before BR injection, 25 min after BR injection, and 3, 7 and 14 days after BR injection. Structural

B-scan transformation produced the following images: I) phase-variance (motion), II) structural B-scan, III) angiographic B-scan, and IV) structural *en face* projections of the imaged region. Additionally, a verification of stroke appearance was made by brightfield camera (Fig. 2SB, 2SC).

Histology

Histological staining was performed 14 days after the stroke induction. The mice were deeply anesthetized with pentobarbital and perfused with warm (37°C) phosphate-buffered saline (PBS) for 5 min followed by 4% paraformaldehyde in PBS for 15 min (at room temperature). The brains were postfixed overnight in the same fixative solution and then transferred to 30% sucrose in 0.01M PBS and kept in a refrigerator for 3-5 days. Serial sections were cut at 40-µm intervals in the coronal plane using a freezing microtome, then transferred to the PBS.

Hematoxylin/eosin (HE) staining

Sections were mounted on SuperFrost (Fisher Scientific, Hampton, New Hampshire, USA) slides and air dried on a slide warmer at 58°C for at least 30 min. Following this, the sections were hydrated by passage through water baths with decreasing alcohol concentrations (2 min in each bath of 100%, 80%, or 50% alcohol and water), stained in Mayer's hematoxylin (Diapath, Martinengo, Italy) for 6 min, and washed in running tap water for 5 min. Next, the slides were stained in Shandon Eosin Y (Thermo Fischer Scientific, Waltham, Massachusetts, USA) for 2 min, washed in tap water for 2 min, dehydrated in baths with increasing alcohol concentrations (1 min in each bath of 50%, 80%, and 100% alcohol), and cleared in xylene. Finally, the sections were mounted in Shandon Consul-Mount media (Thermo Fischer Scientific), which is a non-aqueous, non-fluorescent plastic mounting medium.

Fluoro-Jade staining

Tissue sections for Fluoro-Jade (FJ) staining were mounted on slides, dried and immersed in 1% sodium hydroxide in 80% alcohol. Then sections were immersed in 70% alcohol for 2 min, 50% alcohol for 2 min, and distilled water for 2 min. Next, the slides were incubated in 0.06% potassium permanganate solution for 10 min, rinsed in distilled water for 2 min, and stained with FJ (final concentration, 0.0004% in a 0.1% acetic acid vehicle). After 20 min the slides were rinsed for 3×1 min in distilled water and then placed on a slide warmer set to ~50°C until fully dry (5 to 10 min). The dry slides were cleared by immersion in xylene for at least 1 min and coverslipped with Shandon Consul-Mount.

Immunohistochemistry

Sections were blocked with normal donkey serum (NDS), and after being washed in PBS were incubated in 0.1% Triton X-100 in PBS (PBST) for 15 min. Then, after 1-hour preincubation in 5% NDS-PBST, the following I-order antibodies (Ab) were added (all from Abcam, Cambridge, UK) for overnight incubation at 4°C: goat anti-Iba-1 (1:500) and chicken anti-glial fibrillary acid protein (GFAP) (1:800). After a thorough wash in PBST, sections were incubated for 2 h at room temperature with secondary donkey antibodies (1:400) conjugated to the following fluorochromes (Jackson ImmunoResearch, West Grove, PA): 488 Dylight to detect GFAP and 647 Alexa Fluor to detect Iba-1. After washing in PBST, sections were incubated in Hoechst blue/PBS (Invitrogen, Carlsbad, CA) at a concentration of 20 µg/mL for 15 min and rinsed in PBST. Images of Iba-1/GFAP/Hoechst stain present in the ischemic region were acquired with a fluorescence microscope (Olympus) using VS-ASW-S5 software under a 20× objective (10×10 total magnification). Scanned images were then processed with ImageJ. Hoechst, Iba-1 and GFAP immunocytochemical stains were performed on one 40 µm section (triple staining), and FJ and HE staining were performed on adjacent sections.

Measurements of angiogenesis and gliosis

Based on an OCT *en face* angiographic projection (depth 0–400 µm) taken 25 min after the stroke induction, the area with reduced blood flow by about 85% was delimited. Then, for that area we calculated percentages of both newly formed and reperfused vessels, vessels branches total length, numbers of branches, junctions, and end-points of vessels in ImageJ before the induced stroke, and 25 min, 3, 7, and 14 days after the stroke. (ImageJ steps of the vasculature processing: brightness/contrast – auto, auto-threshold followed by minimal manual threshold correction. Additionally for branches length, numbers of branches, junctions and end-points, we applied plugin Skeleton/Skeletonize 2D/3D). Manual correction was necessary

because in the OCT images the background was heterogeneous at individual days of observation. That heterogeneity of the background was due to inability to position the mice in the same OCT system on each day of imaging. Area of gliosis was defined arbitrarily as an area with hyporeflective OCT signal on structural *en face* projections taken at depth levels from 200 μm to 400 μm. Percentage area of the gliosis was counted in ImageJ for 3, 7, and 14 days after the stroke. Each mouse gliosis surface area was normalized to 100%, corresponding to the result on day 3. We checked for correlations between the sizes of gliosis on immunochemical stained sections and on OCT images at the same depth (400 μm). The width of the core of microgliosis (Iba-1) was compared with the width of the dark core on the OCT structural *en face* projection. The width of the core of astrogliosis (GFAP) was compared with the width of the bright halo on the OCT structural *en face* projection.

Statistical analysis

Wilcoxon signed-rank one-tailed t tests (alpha=0.05) were used to compare area of ischemic core and area of vessels, total length of the vessel branches, number of branches, junctions and end-points between time-points: before the induced stroke and 25 min, 3 days, 7 days and 14 days after the stroke induction. The same statistical test was used to compare the width of microgliosis and astrogliosis staining with the width of the ischemic core and envelope (respectively) observed in the *en face* OCT structural images.

RESULTS

The ischemic area was analyzed at four time points (25 min, 3 days, 7 days, 14 days) by determining the hyporeflective area, called here the "stroke core" (SC), on the various images: *en face* OCT structural projections, b-scans, angiomaps, and angio-b-scans. In the structural images, this characteristic hyporeflective area was observed in the center of the ischemic location. The SC was clearly visible from day 3 onward and then decreased in size until day 14 (Fig. 1C-E, 1H-J). In contrast, immediately after stroke (25 min time point), the SC was not visible on OCT reconstructions (Fig. 1B, 1G). Another effect of reduced blood flow was observed on angiomaps in the center of the ischemic location immediately after green laser irradiation, visible as a dark area between 200 and 500 μm in diameter (mean 355 μm, n=9), devoid of blood flow signal (Fig. 1L). Within the next 14 days more vessels appeared, associated with increasing blood flow due to angiogenesis and reperfusion (Fig. 1M-O). Angio-b-scans revealed that up to 7 days the signal from blood flow was mainly present in the superficial layers of the cortex, while at day 14 the signal was visible also in the deeper part of the cortex (Fig. 1T).

Based on the structural *en face* projections, the area of the ischemic core was measured on days 3, 7 and 14. It was found that the area of SC differed significantly between consecutive days. The largest area was observed on day 3 and the smallest on day 14 (Fig. 2A). Also, changes in vascularization of the infarct area were assessed at time points 25 min, 3, 7, and 14 days (Fig. 2B-F). The reference area was the one where the flow was almost completely stopped (Fig. 4G, 25 min). There was a significant increase in angiogenesis on day 3 and day 7. Similarly, for these days we observed an increase in the branch length (Fig. 2C) and the number of endpoints (Fig. 2F). For the number of branches (Fig. 2D) and the number of junctions (Fig. 2E) a significant increase was only found on day 7. However, between days 7 and 14, angiogenesis was diminished (not statistically significant). It was interesting to focus on the position of a certain small vessel, shown on the angiomap by the white arrow in Fig. 2G), 25 min. This vessel initially formed a clearly visible loop, which then became distended on day 3, and by day 14 it was clearly elongated (Fig. 2G).

Then we determined which elements of nervous tissue correspond to the SC identified on the OCT structural images (Fig. 3). Basic HE histological staining of the brains of 7 mice performed on day 14 revealed densely packed cells at the center of the ischemic region (Fig. 3C). Most of the cells had intensely stained, irregular nuclei with a narrow band of cytoplasm. The size of this area was similar to the size of the dark core visible on structural *en face* projections (Fig. 3B) and b-scans (Fig. 3E). However, in 3 mice with minor stroke (Fig. 3G), HE staining showed no clear area with densely dark-stained cells in the center of the infarct on day 14, as it was with the other mice (Fig. 3L). Also on the structural *en face* projections (Fig. 3H) and b-scans (Fig. 3K) no dark area was observed. In some mice on the *en face* structural projection we observed a clear light halo with a granular structure localized around the dark core (Fig. 3B), which was less visible on a single b-scan (Fig. 3E).

In order to further identify the elements of the nervous tissue located in the ischemic area, in the center of the infarct and in its bright halo, we performed immunocytochemical staining for the presence of microglia/macrophages (Iba-1), astrocytes (GFAP), nuclei of neurons and glia (Hoechst), and degenerating

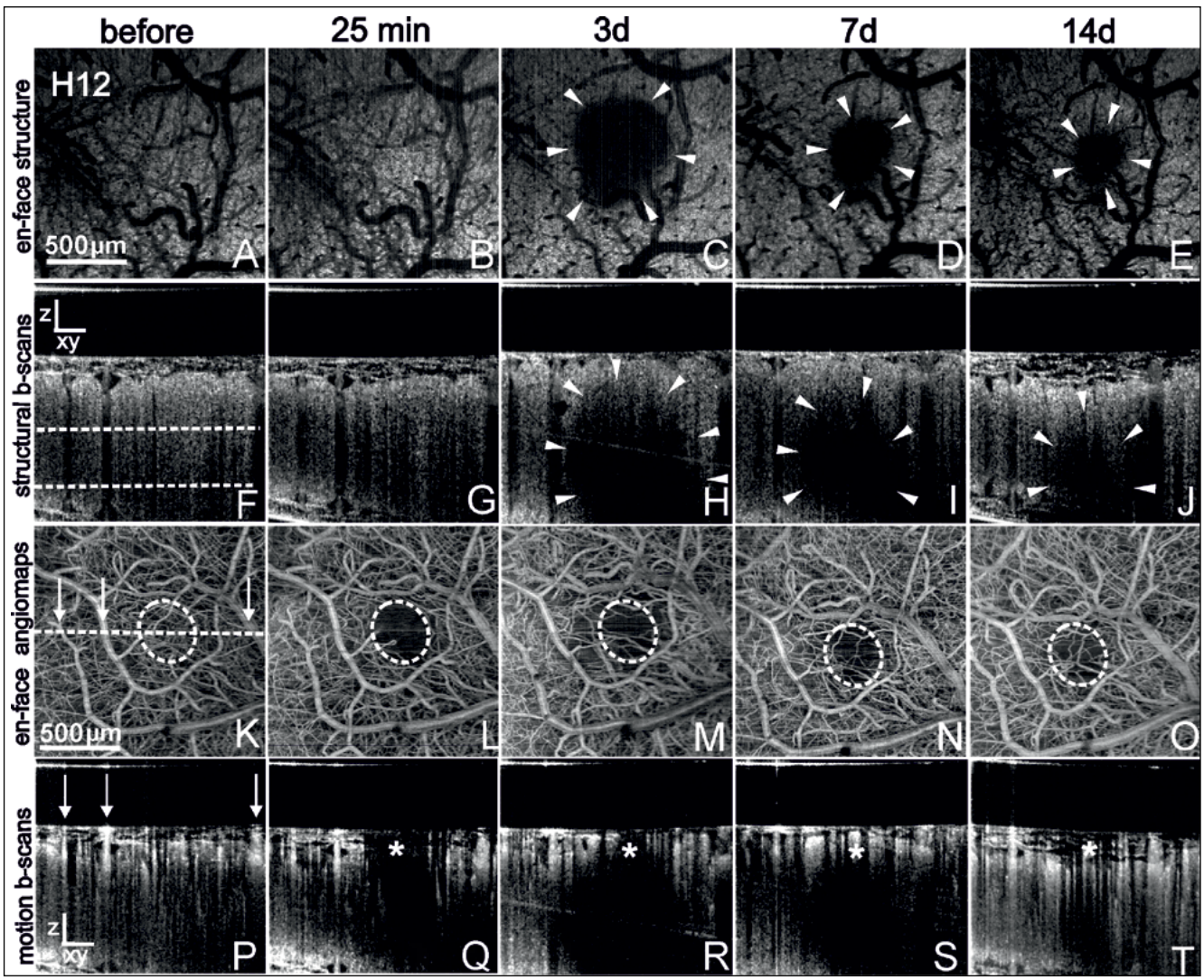

Fig. 1. OCT images demonstrating the ischemic region during the course of 14 days. (A-E) The *en face* structural images showed that from day 3 to day 14, a hyporeflective SC (marked by arrowheads) was visible, which gradually decreased until day 14. (F-J) The same dark core was seen in the structural b-scans, with the dashed lines indicating the cortical depths taken for the structural *en face* images. (K-O) Angiomaps showing the presence of a dark center of ischemia bounded by a dashed line (zoom-in of the circular ROI is presented at Fig. 4G). (P-T) b-scans taken from the center of the ischemic area (dashed line in k). The star shows the central part of the stroke, and the arrows indicate the position of the large vessels, as in the above angiomap. Scale bar: z=100 µm, xy=200 µm.

neurons (Fluoro Jade B). The staining is shown in Fig. 6 using the H13 mouse as an example. The corresponding OCT images scanned in the H13 mouse are shown in Fig. 3B, E). Hoechst staining showed that the center of the infarct is occupied by densely packed nuclei (Fig. 4A), corresponding to the region with dark stained and densely packed HE cells (Fig. 3C). Staining for the Iba-1 protein mainly showed the presence of activated amoeboid microglia/macrophages in this region (Fig. 4B). Thus, it seems that the dark core visible on the structural images is formed mainly by the activated microglia/macrophages. On the other hand, the bright halo around the SC, visible in the OCT structural images, corresponds to the area with lower cell density, visible with the Hoechst and HE stains. Staining for the GFAP protein revealed that the halo was mainly occupied by hypertrophic astrocytes with numerous long processes (Fig. 4C). Also, numerous FJ degenerating neurons were detected in the halo area. In contrast, in the core there were few FJ neurons (Fig. 4D). We found that the halo was absent in those strokes where there was only a small amount of activated astrocytes in the OCT imaging area (depth 0–400 µm), as is exemplified by mouse H12 (Fig. 1), in which the astrocytes were located primarily below 400 µm. In mice with minor strokes, where no OCT SC nor bright halo

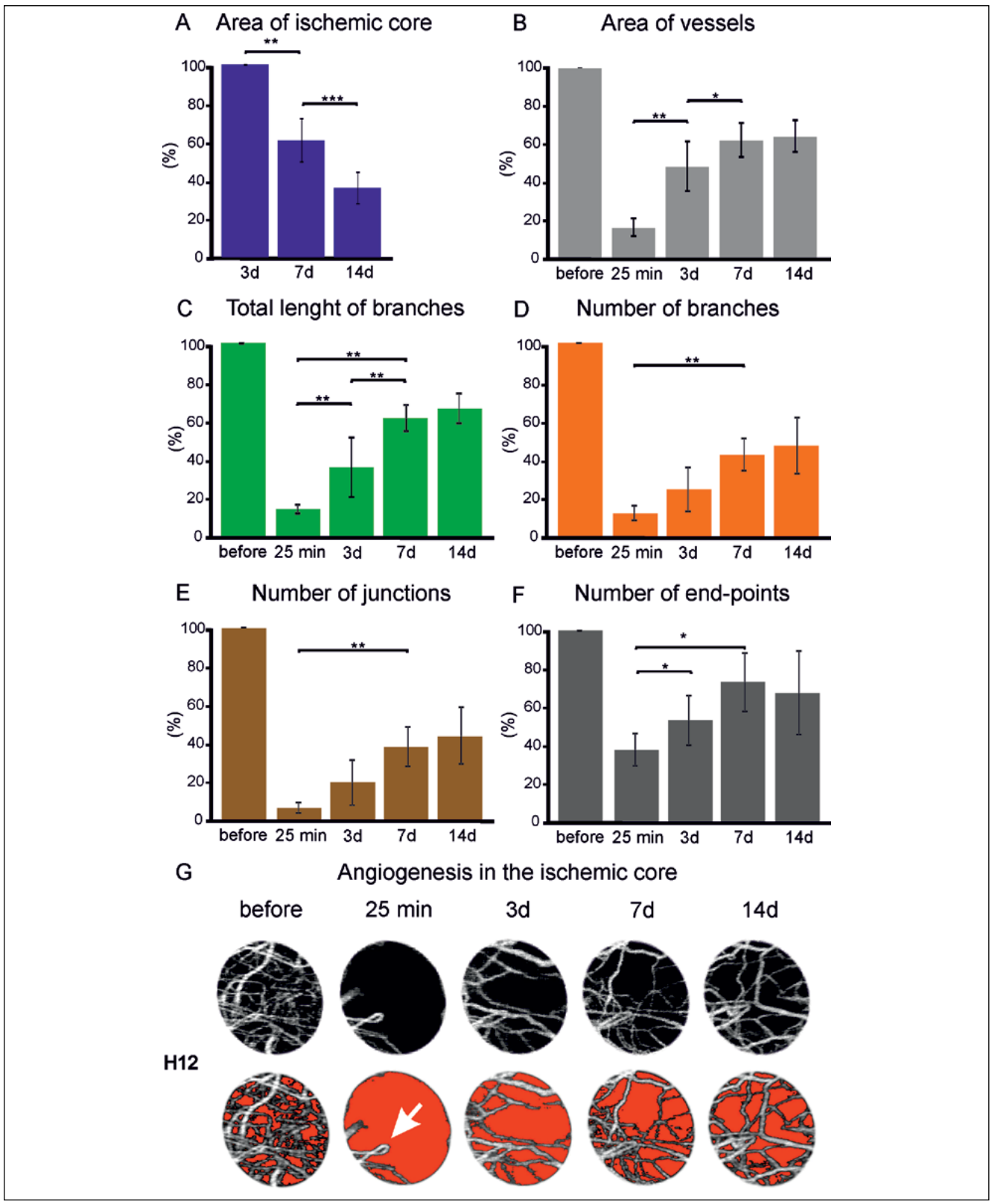

Fig. 2. Quantitative analysis of the ischemic region during 14 days. (A) Surface area of the dark core visible on *en face* structural projections (n=7). (B-F) Measurements of five parameters characterizing vasculature of the central part of the ischemic region in comparison to the values before the stroke (n=6). (G) Magnified example of the SC is presented from mouse H12. Upper row – original OCT image of ischemic core. Lower row – ischemic core after thresholding (ImageJ). Error bars present standard deviation, * $P \leq 0.05$, ** $P \leq 0.01$, *** $P \leq 0.001$ (Wilcoxon test).

was observed, staining for Iba-1 showed no presence of densely packed activated microglia/macrophage cells (Fig. 4F), and GFAP staining showed no presence of hypertrophic astrocytes in the area of ischemia (Fig. 4G). FJ degenerating neurons were present at the center of the infarct (Fig. 4H).

Observations that the dark SC on the OCT projection is mainly occupied by densely packed microg-

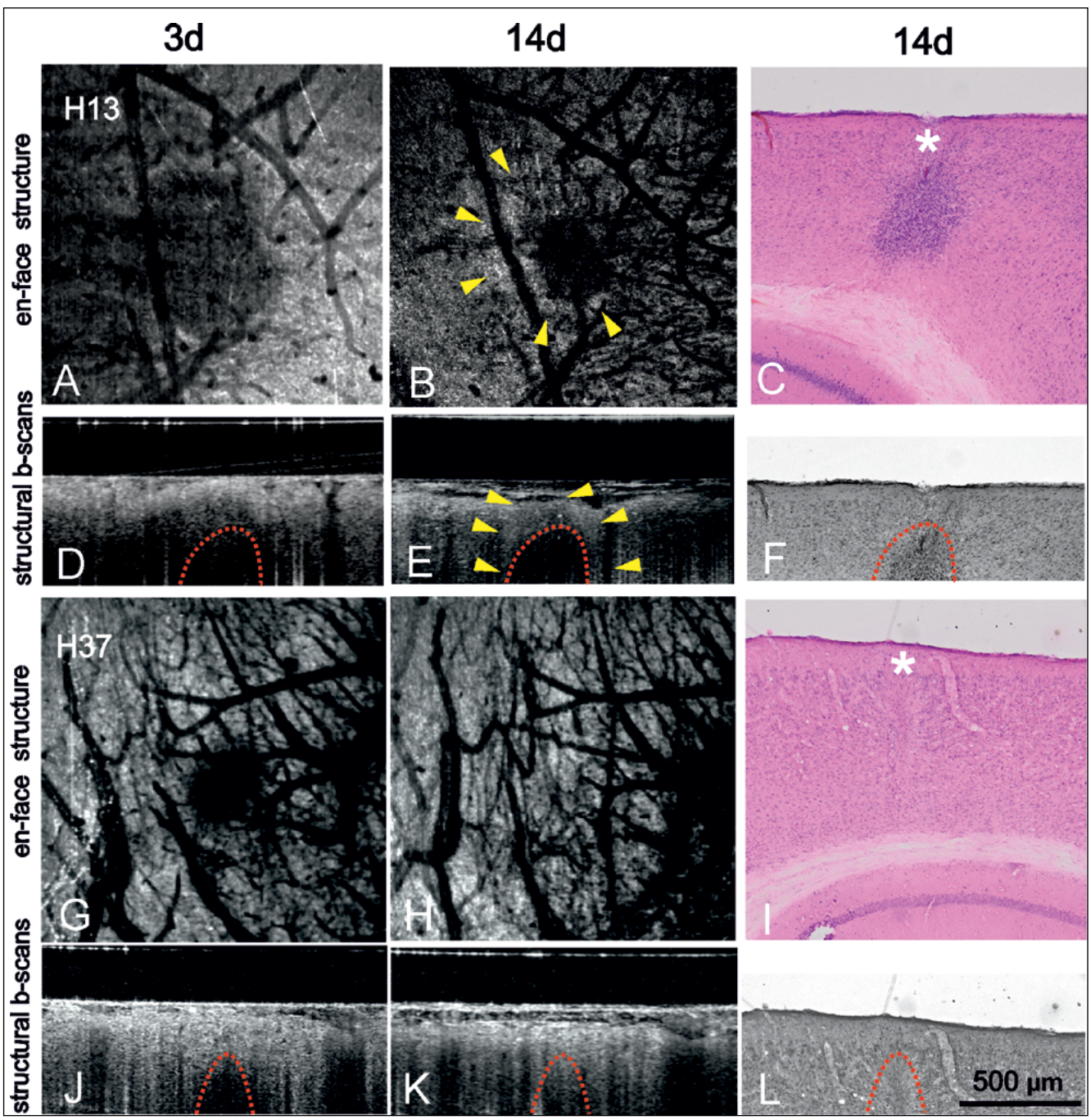

Fig. 3. Comparison of the SC visible on the structural OCT images with HE staining in two representative mice (H13, H37). OCT images show the appearance of the ischemic area at day 3 (A, D, G, J). The size of the core on *en face* structural projection (B) and structural b-scans (E) at day 14 in mouse H13 correlated with the size of the region occupied by darkly HE-stained and densely packed cells in the center of the ischemic region. In mouse H37, the lack of a dark area (H, K) corresponded to the lack of darkly HE-stained and densely packed cells (I, L). Red dotted line delimits the dark core, and yellow arrowheads indicate the bright halo surrounding the dark core. White stars demarcate the ischemic region on HE sections (C, I).

lia/macrophages and enveloped by astrocytes were confirmed quantitatively. We found that the width of the core of the microgliosis did not differ from the width of the dark core visible on the OCT structural projections (Fig. 4I). Similarly, the width of astrogliosis measured on GFAP-stained sections did not differ from the width of the bright halo on OCT images (Fig. 4I).

With the example of a shallow stroke (mouse H6), limited to the cortex depth of approx. 400 µm, cells in the bright halo were analyzed in detail. On two *en face* structural levels from 100 µm (Fig. 5A) and

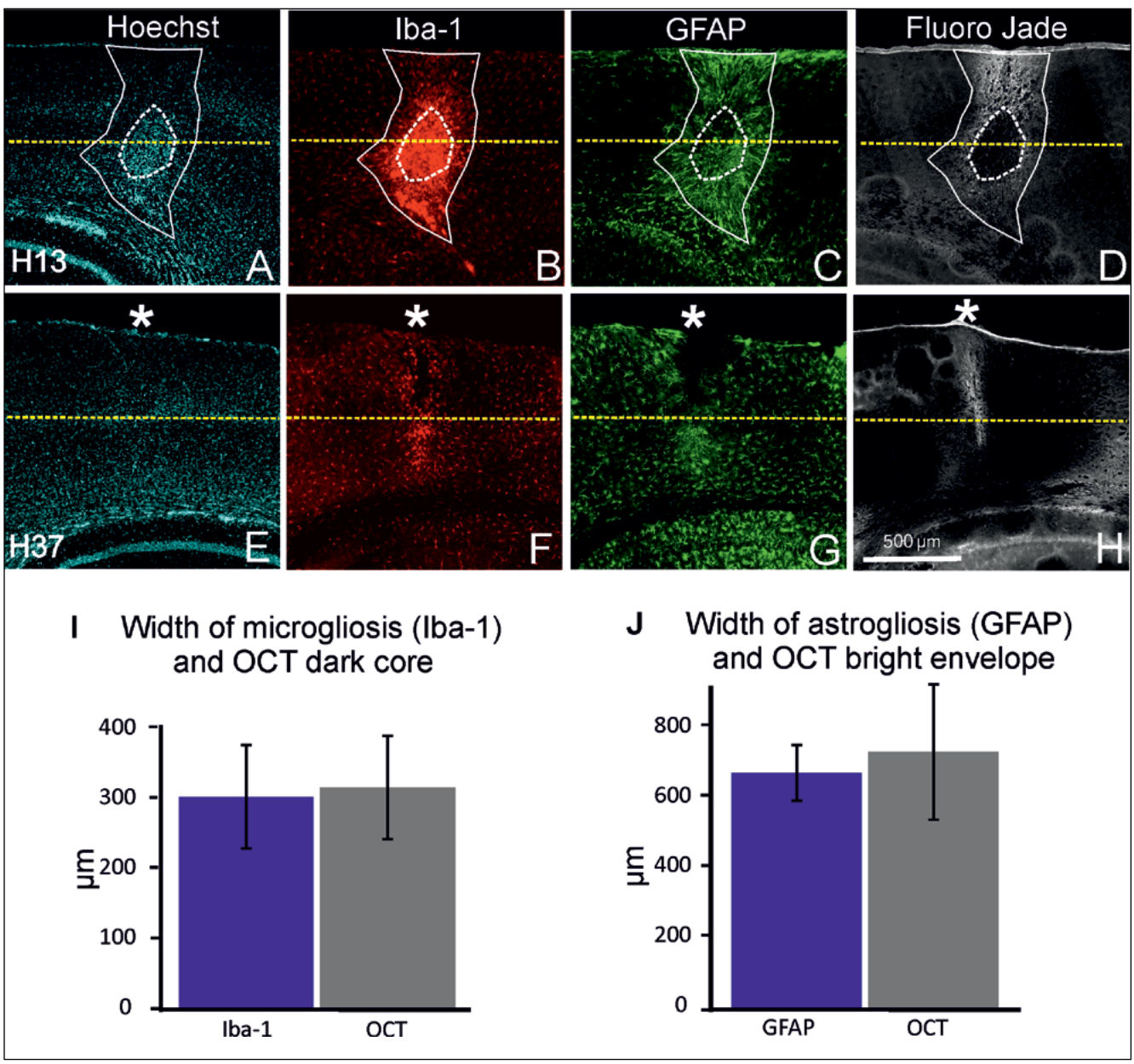

Fig. 4. Immunocytochemical staining of the ischemic region in two representative mice (H13, H37) at day 14. In the representative mouse with a large stroke (H13), the ischemic core was occupied by densely packed microglia/macrophages (A, B). The dotted white line delimits the group of densely arranged nuclei of neurons and glia stained by Hoechst's method. Astrocytes (C) and degenerating neurons (D) were localized mainly in the halo region. A solid white line was initially marked in the GFAP image and demarcates the area with hypertrophic astroglial processes. A representative mouse with a small stroke (H37) showed the absence of densely packed microglial cells/macrophages (E, F) and the presence of a few activated astrocytes (G). In the central part, positive FJ degenerative neurons are visible (H). The yellow dotted line indicates the OCT imaging depth (about 450 µm). (I) Quantitative representation of width of microgliosis *vs.* dark core on the OCT images, n=7 (not significant). (J) The width of astrogliosis *vs.* bright halo on OCT images, n=6 (not significant).

200 µm from the brain surface (Fig. 5B), a bright halo was clearly visible around the dark core. Three-dimensional reconstruction from a series of 100 b-scans from the ischemic area also revealed a SC and a distinct light halo with characteristic granularities (Fig. 5C). Immunocytochemical staining confirmed that in the center of the infarct shown on Fig. 5D there were densely arranged cells of activated microglia/macrophages (Fig. 5D), and around them, astrocytes were located in the region corresponding to the OCT bright halo (Fig. 5E), as well as FJ degenerating neurons (Fig. 5F).

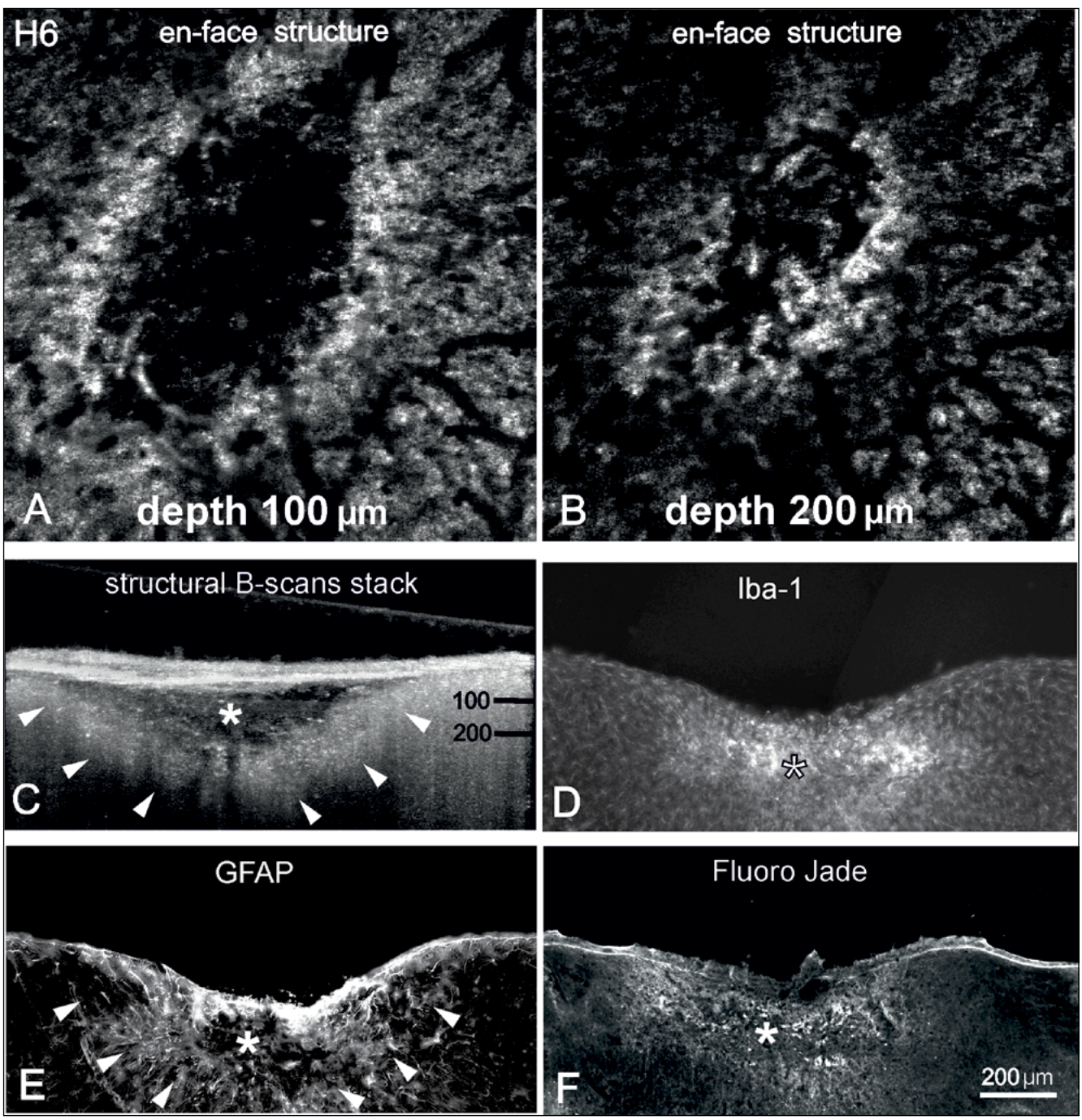

Fig. 5. Example of structural heterogeneity of the ischemic region. (A, B) Structural *en face* projections at different depths and (C) stack of structural b-scans demonstrating distinct bright (white arrowheads) halo around the SC (white star). (D) Staining for Iba-1 showed that the SC (white star) was occupied by microglia/macrophages, whereas halo was occupied by hyperactive astrocytes (white arrowheads) (E) and degenerating neurons (F). Thus, a similar pattern was observed here as was demonstrated in mouse H13 (Fig. 4).

DISCUSSION

The modified OCT system was used both for stroke induction with a green diode laser and for brain imaging with a Gauss beam from an 850 nm laser, with both beams passing through the same objective. This has previously been described and applied using a different system based on a Mach-Zehnder interferometer and using Bessel beams (Doleżyczek et al., 2020a). The currently used system has a different light source – a laser diode (SUPERLUM M-T-850-HP-I), which is more stable than the femtosecond laser (Fusion Femtolasers, Austria) used earlier. Also, a different illumination path was used. This instrument captures images by scanning the Gauss beam, which allows three-dimensional imaging with high resolution (2-3 μm), but the depth of penetration is limited to 450 μm. Therefore, in some cases, only the upper part of the ischemic area was detected. Although our previously used OCT setup with a 795 nm Bessel beam allows almost twice the penetration depth compared to Gauss scanning, the complex interferometer significantly reduced the stability of the measurements (Doleżyczek et al., 2020b).

Some authors have used MRI to visualize changes in the brain in the course of stroke in rodents. With the use of a 1.5-T MRI scanner (Chen et al., 2007), the spatial resolution of the imaging was about 1.5 mm, whereas with a 3-T scanner the resolution was 1 mm (Huang et al., 2019). Even using ultra-high-field MRI (9.5-T), for generating mouse connectome brain atlas, spatial resolution was 45 μm (Wang et al., 2020). Thus, the MRI imaging resolution is many times lower than the OCT resolution (2-3 μm). Due to the fact that the aim of our study was to trace changes in both the brain tissue and the network of blood vessels, including capillaries, in the course of stroke, the choice of OCT is adequate. Other advantages of using OCT are obtaining high-quality images without providing contrast, avoiding the negative effects of electromagnetic field on the organism, and a significantly lower cost of building OCT compared to MRI.

We used a modified phototoxic stroke model in which a focal ischemic area with an average diameter of 355 μm was obtained. The green beam was located on the cerebral cortex to not include large vessels; accordingly, the ischemic area was relatively small and the differences between mice in stroke size were small (300-500 μm). Owing to appropriately selected parameters of the beam diameter, laser power and exposure time, the area of infarct had a preserved cellular structure. In studies of Lu et al. (2020) and Yang et al. (2018, 2019), large lesions over 1 mm in diameter resulted in damage of the core region.

Due to the high robustness of the applied OCT system in the present experiments, it was possible to observe on the structural and angiographic maps the heterogeneity of the ischemic area and its evolution over 2 weeks. We found on the OCT structural *en face* projections and b-scans a distinct SC of strongly hyporeflective OCT signal in the center of the ischemic region, which appeared on the 3rd day after stroke induction and gradually decreased to day 14. Around the periphery of the SC in the OCT structural images the scattered signal was much stronger and visible as a bright halo. A similar pattern of the scattering signal in the ischemic region has been observed before (Srinivasan et al., 2012, Yang et al., 2018, Choi et al., 2019, Park et al., 2020). A bright halo can define a region of penumbra with a glial scar, which mainly consists of activated astrocytes, and it has the function of isolating the infarct region from healthy tissue (Zbesko et al., 2018). Indeed, we showed a correspondence of the pattern of the OCT scattered signal visible on structural images with the arrangement of different types of glia forming the SC and penumbra. Immunocytochemical staining revealed that the main source of the weak scattered signal in the SC appeared to be activated, amoeboid microglia/macrophages, while the bright halo appears to be built mainly from loosely arranged cell bodies and processes of activated, hypertrophic astrocytes. FJ staining also showed the presence of degenerating neurons in the halo.

The physical cause of the increased diffuse signal attenuation is not clear. The presence of a dark core may suggest that an influx of macrophages can alter the refractive index and perhaps block light from reaching deeper layers. The bright halo around this area represents an increase in the scattering signal, which appears to be related to the presence of hypertrophic astroglial processes. On the other hand, a change in tissue structure is also observed on histological sections, which may suggest the rearrangement of the tissue related to the presence of local edema, which usually manifests itself as hyporeflectivity in OCT images. The observed granular nature of the halo, clearly visible on the structural images, may reflect the presence of astroglia and neurons. We found that in those mice where we did not observe the bright halo, staining for GFAP showed no astrocytes at the depth of the OCT scan. Yang at al. (2019), using OAC-OCT in rats, also showed the presence of a SC with a weak scattering signal in the ischemic area and a surrounding area with a stronger signal and a clear bright halo. According to our observations, the halo area identified by Yang et al. (2019) on the border of the ischemic core and penumbra occupied by astrocytes would partially cover the area of activated astrocytes that we iden-

tified by immunocytochemistry in the mouse model. In our experiments, we applied a 4× objective which did not achieve cellular resolution on the OCT images, and as a result the neurons or glial cells could not be clearly identified. The advantage was the ability to image a broad area of the brain around the infarct and a large work distance, ensuring easier mouse manipulation. To visualize neurons, Srinivasan used the system with a 40× water immersion objective (Srinivasan et al., 2012).

It is known from the literature that after ischemic stroke angiogenesis begins in the area of the penumbra, allowing for tissue recovery (Hayashi et al., 2003). In our previous work with the glioblastoma model, we showed that OCT can be used to assess the rate of angiogenesis in a tumor over 14 days (Dolezyczek et al., 2020a). In the present study, we quantified the progression of angiogenesis over 2 weeks, with strong angiogenesis observed on days 3 and 7. Literature data demonstrated that in mice, the first stage of angiogenesis in the area of ischemia is associated with the appearance of dividing endothelial cells as early as 1 day after the stroke. The endothelial cells sprout and form new vessels that are visible from day 3 post-stroke, and intense angiogenesis continues for up to 21 days (Hayashi et al., 2003; Yang et al., 2018). After a stroke, the phenomena of reperfusion and angiogenesis occur at different rates, restoring the optimal level of blood flow in the area of ischemia as a strategy for tissue survival. In some of the vessels, especially in the first hours after a stroke, spontaneous reperfusion occurs (Durand et al., 2012; Doleżyczek et al., 2020b). Analyzing the OCT images, we observed changes in the spatial arrangement of some vessels within 14 days. Similarly, changes in vascular position have been observed by Choi at al. (2019) already in the first hours after stroke, but this is the effect of edema rather than remodeling and angiogenesis. Regarding the analysis of long-term changes in vascularization after stroke presented in the literature, studies by Lu et al. (2020) focused on the assessment of changes in the orientation of vessels in the penumbra area exclusively using the parameters of capillary orientation and capillary stalling event. On the other hand, Yang et al. (2018; 2019) analyzed vessel area density on angiograms to assess the size of the core area in a rat model. Yang et al. (2018) focused on the cortical surface fraction (depth of focus was around 122 μm). Differently, in our study many parameters were used to assess vascularization within the core at a depth of 0-400 μm. Apart from the vessel surface area, the total length and number of branches, and numbers of the junctions and end-points of the vessels branches were also measured.

CONCLUSION

Using a prototype OCT system and a photo-induced mice stroke model, we revealed a heterogeneous OCT signal pattern in the ischemic area that changed over 2 weeks. In structural OCT *en face* projections and b-scans, we found a distinct SC with a hyporeflective signal in the center of the ischemic area, which appeared on day 3 after green laser irradiation and gradually decreased until day 14. Also, angiomaps showed the presence of the SC in the center of the ischemia; however, it was smaller than the dark areas in the structural images. This distinction suggests a different tissue source of the scattered signal. We observed a bright halo on the OCT structural images around the dark SC region. Immunocytochemical staining revealed that the main source of the weak scattered signal in the ischemic core appeared to be activated, amoeboid microglia/macrophages while the stronger scattering signal from the bright halo appeared to be from activated, hypertrophic astrocytes. The surface area of gliosis reflected by the SC on the OCT *en face* structure decreased by 70% between days 3 and 14. Angiogenesis measured by the surface area of vessels located in the center of the ischemia increased significantly by day 7 after stroke induction. This was especially the case on day 3, when it increased twice compared to the initial observation at 25 min.

ACKNOWLEDGEMENTS

The execution of this experiment was supported by the International Centre for Translational Eye Research (MAB/2019/12) project, carried out within the International Research Agendas Programme of the Foundation for Polish Science, co-financed by the European Union under the European Regional Development Fund. National Science Center (NCN, 2016/22/A/ST2/00313); European Union's Horizon 2020: research and innovation programme (666295); Polish National Agency for Academic Exchange (PPN/PPO/2018/1/00082) and Polish Ministry of Science and Higher Education (2016-2019 int.) co-financed project. JW acknowledge the National Science Centre grant number 2017/26/E/NZ4/00637.

REFERENCES

Baumann B, Woehrer A, Ricken G, Augustin M, Mitter C, Pircher M, Kovacs GG, Hitzenberger CK (2017) Visualization of neuritic plaques in Alzheimer's disease by polarization-sensitive optical coherence microscopy. Sci Rep 7: 43477.

Bosetti F, Koenig JI, Ayata C, Back SA, Becker K, Broderick JP, Carmichael ST, Cho S, Cipolla MJ, Corbett D, Corriveau RA, Cramer SC, Ferguson AR, Finklestein SP, Ford BD, Furie KL, Hemmen TM, Iadecola C, Jakeman LB, Janis S, Jauch EC, Johnston KC, Kochanek PM, Kohn H, Lo EH, Lyden PD, Mallard C, McCullough LD, McGavern LM, Meschia JF, Moy CS, Perez-Pinzon MA, Ramadan I, Savitz SI, Schwamm LH, Steinberg GK, Stenzel-Poore MP, Tymianski M, Warach S, Wechsler LR, Zhang JH, Koroshetz W (2017) Translational stroke research: vision and opportunities. Stroke 48: 2632–2637.

Chen F, Suzuki Y, Nagai N, Jin L, Yu J, Wang H, Marchal G, Ni Y (2007) Rodent stroke induced by photochemical occlusion of proximal middle cerebral artery: evolution monitored with MR imaging and histopathology. Eur J Radiol 63: 68–75.

Choi WJ, Li Y, Wang RK (2019) Monitoring acute stroke progression: multi-parametric OCT imaging of cortical perfusion, flow, and tissue scattering in a mouse model of permanent focal ischemia. IEEE Trans Med Imaging 38: 1427–1437.

Desissaire S, Pollreisz A, Sedova A, Hajdu D, Datlinger F, Steiner S, Vass C, Schwarzhans F, Fischer G, Pircher M, Schmidt-Erfurth U, Hitzenberger C (2020) Analysis of retinal nerve fiber layer birefringence in patients with glaucoma and diabetic retinopathy by polarization sensitive OCT. Biomed Opt Express 11: 5488–5505.

Dirnagl U, Iadecola C, Moskowitz MA (1999) Pathobiology of ischemic stroke: an integrated view. Trends Neurosci 22: 391–397.

Dolezyczek H, Rapolu M, Niedzwiedziuk P, Karnowski K, Borycki D, Dzwonek J, Wilczynski G, Malinowska M, and Wojtkowski M (2020a) Longitudinal *in-vivo* OCM imaging of glioblastoma development in the mouse brain. Biomed Opt Express 11: 5003–5016.

Dolezyczek H, Tamborski S, Majka P, Sampson DM, Wojtkowski M, Wilczynski G, Szkulmowski M, Malinowska M (2020b) In vivo brain imaging with multimodal optical coherence microscopy in a mouse model of thromboembolic photochemical stroke. Neurophoton 7: 015002.

Durand A, Chauveau F, Cho TH, Bolbos R, Langlois JB, Hermitte L, Wiart M, Berthezène Y, Nighoghossian N (2012) Spontaneous reperfusion after in situ thromboembolic stroke in mice. PloS One 7: e50083.

Gesperger J, Lichtenegger A, Roetzer T, Salas M, Eugui P, Harper DJ, Merkle CW, Augustin M, Kiesel B, Mercea PA, Widhalm G, Baumann B, Woehrer A (2020) Improved diagnostic imaging of brain tumors by multimodal microscopy and deep learning. Cancers 12: 1806.

Hatakeyama M, Ninomiya I, Kanazawa M (2020) Angiogenesis and neuronal remodeling after ischemic stroke. Neural Regen Res 15: 16–19.

Hayashi T, Noshita N, Sugawara T, Chan PH (2003) Temporal profile of angiogenesis and expression of related genes in the brain after ischemia. J Cereb Blood Flow Metab 23: 166–180.

Hee MR, Baumal CR, Puliafito CA, Duker JS, Reichel E, Wilkins JR, Coker JG, Schuman JS, Swanson EA, Fujimoto JG (1996) Optical coherence tomography of age-related macular degeneration and choroidal neovascularization. Ophthalmology 103: 1260–1270.

Huang WY, Wu G, Guo SX, Geng DY, Li JJ, Yang K (2019) Multi-parameters of magnetic resonance imaging to estimate ischemia-reperfusion injury after stroke in hyperglycemic rats. Sci Rep 9: 2852.

Lee J, Gursoy-Ozdemi Y, Fu B, Boas DA, Dalkara T (2019) Optical coherence tomography imaging of capillary reperfusion after ischemic stroke. Appl Opt 55: 9526–9531.

Lee RH, Lee MH, Wu CY, Couto e Silva A, Possoit HE, Hsieh TH, Minagar A, Lin HW (2018) Cerebral ischemia and neuroregeneration. Neural Regen Res 13: 373–385.

Lu Y, Lu X, Zhang C, Marchand PJ, Lesage F (2020) Longitudinal optical coherence tomography imaging of tissue repair and microvasculature regeneration and function after targeted cerebral ischemia. J Biomed Opt 25: 046002.

Mărgăritescu O, Mogoantă L, Pirici I, Pirici D, Cernea D, Mărgăritescu C (2009) Histopathological changes in acute ischemic stroke. Rom J Morphol Embryol 50: 327–339.

Osiac E, Bălşeanu TA, Mogoantă L, Gheonea DI, Pirici I, Iancău M, Mitran SI, Albu CV, Cătălin B, Sfredel V (2014) Optical coherence tomography investigation of ischemic stroke inside a rodent model. Rom J Morphol Embryol 55: 767–772.

Paciaroni M, Caso V, Agnelli G (2009) The concept of ischemic penumbra in acute stroke and therapeutic opportunities. Eur Neurol 61: 321–330.

Park KS, Shin JG, Qureshi MM, Chung E, Eom TJ (2018) Deep brain optical coherence tomography angiography in mice: in vivo, noninvasive imaging of hippocampal formation. Sci Rep 8: 11614.

Park KS, Ki JW, Lee BH, Eom TJ (2020) Angiographic imaging of an in vivo mouse brain as a guiding star for automatic digital refocusing in OCT. Appl Sci 10: 1210.

Schilling M, Besselmann M, Müller M, Strecker JK, Be Ringelstein E, Kiefer R (2005) Predominant phagocytic activity of resident microglia over hematogenous macrophages following transient focal cerebral ischemia. An investigation using green fluorescent protein transgenic bone marrow chimeric mice. Exp Neurol 196: 290–297.

Srinivasan VJ, Radhakrishnan H, Jiang JY, Barry S, Cable AE (2012) Optical coherence microscopy for deep tissue imaging of the cerebral cortex with intrinsic contrast. Opt Express 20: 2220–2239.

Srinivasan VJ, Mandeville ET, Can A, Blasi F, Climov M, Daneshmand A, Hyun Lee J, Yu E, Radhakrishnan H, Lo EH, Sakadžić S, Eikermann-Haerter K, Ayata C (2013) Multiparametric, longitudinal optical coherence tomography imaging reveals acute injury and chronic recovery in experimental ischemic stroke. PloS One 8: e71478.

Sunil S, Evren Erdener S, Cheng X, Kura S, Tang J, Jiang J, Karrobi K, Kılıç K, Roblyer D, Boas DA (2021) Stroke core revealed by tissue scattering using spatial frequency domain imaging. Neuroimage Clin 29: 102539.

Tamborski S, Lyu HC, Dolezyczek H, Malinowska M, Wilczynski G, Szlag D, Lasser T, Wojtkowski M, Szkulmowski M (2016) Extended-focus optical coherence microscopy for high-resolution imaging of the murine brain. Biomed Opt Express 7: 4400–4414.

Wang N, Anderson RJ, Ashbrook DG, Gopalakrishnan V, Park Y, Priebe CE, Qi Y, Laoprasert R, Vogelstein JT, Williams RW, Johnson GA (2020) Variability and heritability of mouse brain structure: Microscopic MRI atlases and connectomes for diverse strains. Neuroimage 15: 117274.

Yang S, Liu K, Ding H, Gao H, Zheng X, Ding Z, Xu K, Li P (2018) Longitudinal in vivo intrinsic optical imaging of cortical blood perfusion and tissue damage in focal photothrombosis stroke model. J Cereb Blood Flow Metab 39: 1381–1393.

Yang S, Liu K, Yao L, Liu K, W Geng, Xu K, Li P (2019) Correlation of optical attenuation coefficient estimated using optical coherence tomography with changes in astrocytes and neurons in a chronic photothrombosis stroke model. Biomed Opt Express 10: 6258–6271.

Yecies D, Liba O, SoRelle ED, Dutta R, Yuan E, Vogel H, Grant GA, de la Zerda A (2019) Speckle modulation enables high-resolution wide-field human brain tumor margin detection and in vivo murine neuroimaging. Sci Rep 9: 10388.

Zbesko JC, Nguyen TV, Yang T, Frye JB, Hussain O, Hayes M, Chung A, Day WA, Stepanovic K, Krumberger M, Mona J, Longo FM, Doyle KP (2018) Glial scars are permeable to the neurotoxic environment of chronic stroke infarcts. Neurobiol Dis 112: 63–78.

SUPPLEMENTAL MATERIALS

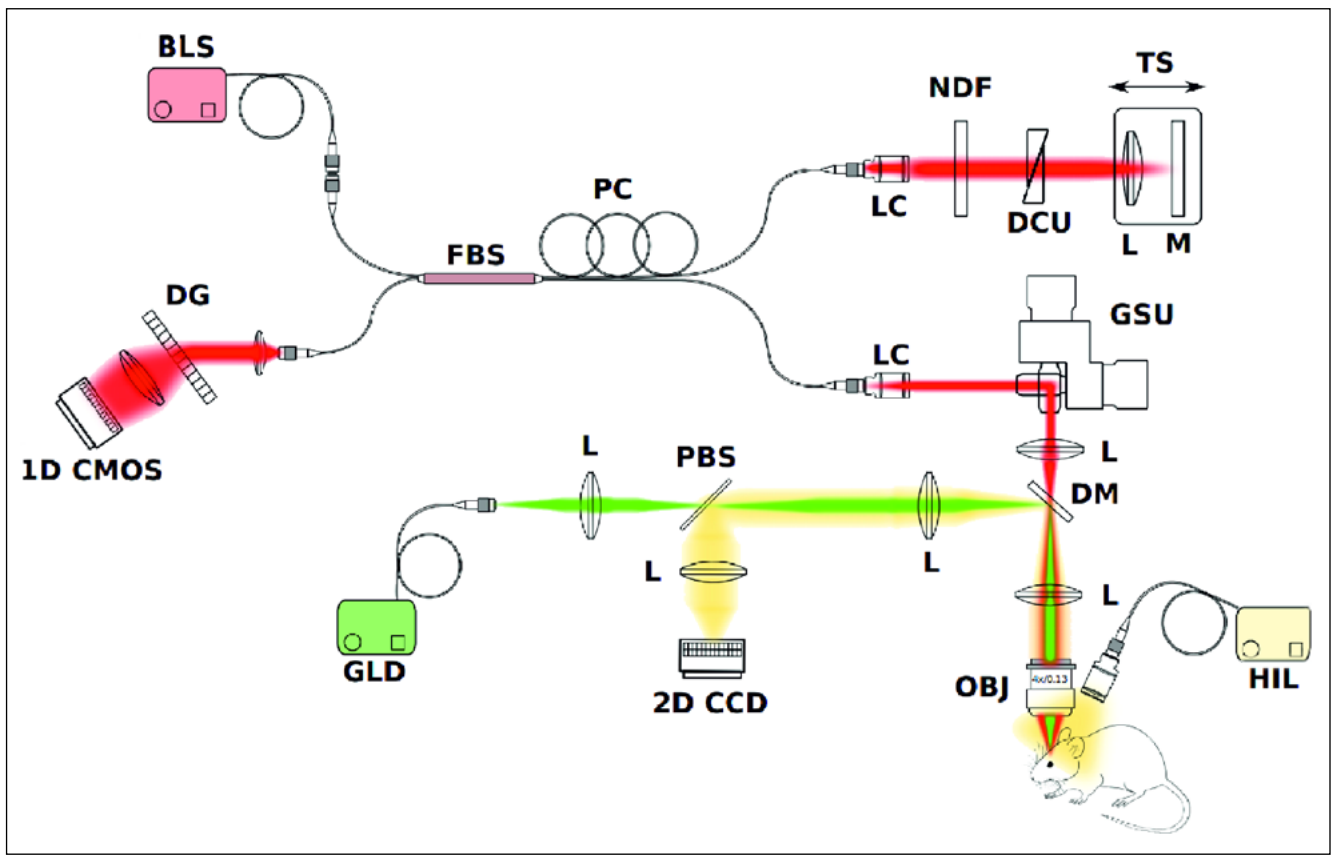

Fig. 1S. Multifunctional OCT system for stroke induction and brain imaging: BLS, broadband light source; HIL, halogen illuminator; GLD, green laser diode; OBJ, objective lens; DM, dichroic mirror; GSU, galvanometric scanning unit; LC, light collimator; PC, polarization controller; NDF, gradient density neutral filter; DCU, dispersion control unit; FBS, fiber beamsplitter; 1-D CMOS, line-scan camera; PBS, pellicle beamsplitters; 2-D CCD, array CCD camera. Color coding for beam path: Gaussian OCT beam (red), brightfield detection (yellow), focal stroke photoinduction illumination (green).

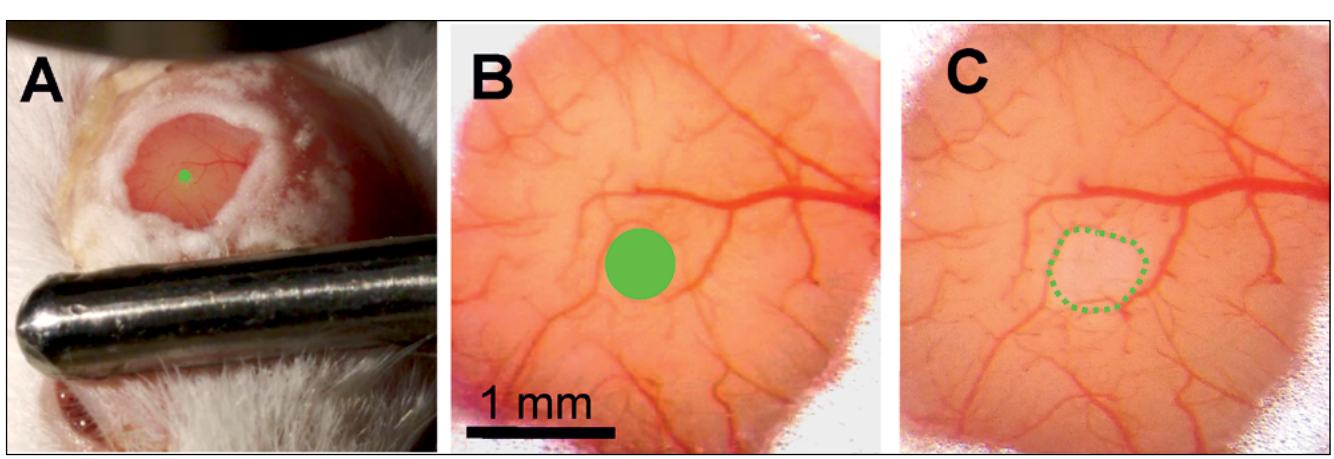

Fig. 2S. Induction of the photostroke by green laser illumination. (A) Localization of the laser beam on the cortex surface visible throughout the cranial window. (B) Green circle indicates laser beam location. (C) Area after 25 min of illumination. The green dotted line delimits tissue with limited blood flow.